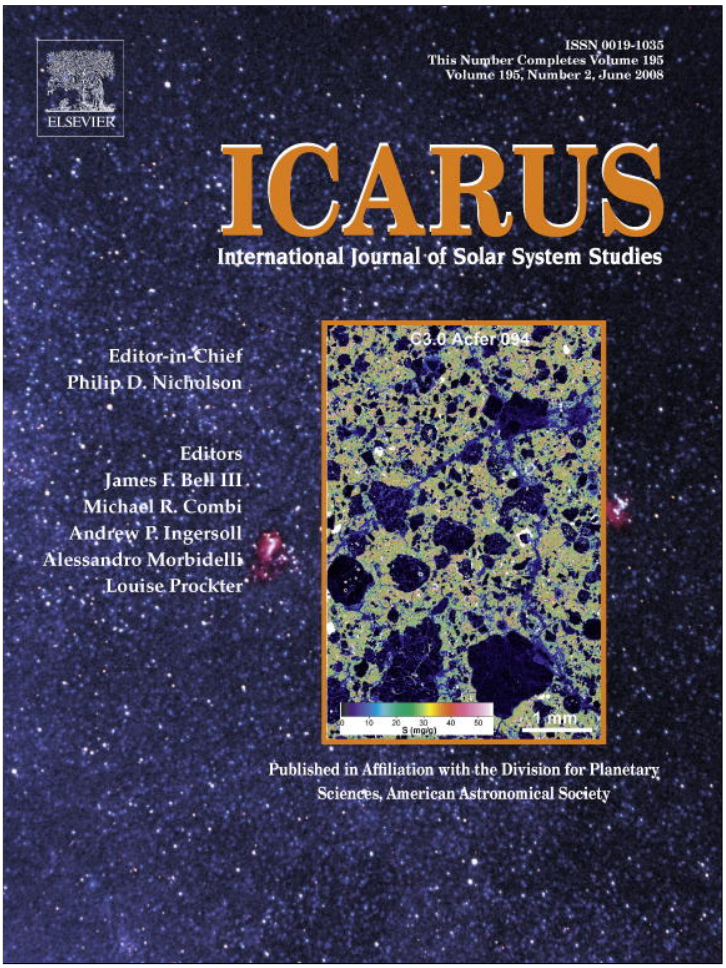

Available online at www.sciencedirect.com
ScienceDirect
Icarus 195 (2008) 547–556
ICARUS
www.elsevier.com/locate/icarus

Simultaneous mapping of H_2O and H_2O_2 on Mars from infrared high-resolution imaging spectroscopy

T. Encrenaz [a,*], T.K. Greathouse [b], M.J. Richter [c], B. Bézard [a], T. Fouchet [a], F. Lefèvre [d], F. Montmessin [d], F. Forget [e], S. Lebonnois [e], S.K. Atreya [f]

[a] *LESIA, Observatoire de Paris, CNRS, UPMC, Université Paris Diderot, 92195 Meudon, France*
[b] *Southwest Research Institute, Div. #15, San Antonio, TX 78228, USA*
[c] *Physics Department, University of California, Davis, CA 95616, USA*
[d] *Service d'Aéronomie, 5 place Jussieu, 75231 Paris cedex 05, France*
[e] *Laboratoire de Météorologie Dynamique, 5 place Jussieu, 75231 Paris cedex 05, France*
[f] *Department of Atmospheric, Oceanic and Space Sciences, University of Michigan, Ann Arbor, MI 48109-2143, USA*

Received 26 December 2006; revised 21 December 2007

Available online 4 March 2008

Abstract

New maps of martian water vapor and hydrogen peroxide have been obtained in November–December 2005, using the Texas Echelon Cross Echelle Spectrograph (TEXES) at the NASA Infra Red Telescope facility (IRTF) at Mauna Kea Observatory. The solar longitude L_s was 332° (end of southern summer). Data have been obtained at 1235–1243 cm^{-1}, with a spectral resolution of 0.016 cm^{-1} ($R = 8 \times 10^4$). The mean water vapor mixing ratio in the region [0°–55° S; 345°–45° W], at the evening limb, is 150 ± 50 ppm (corresponding to a column density of 8.3 ± 2.8 pr-μm). The mean water vapor abundance derived from our measurements is in global overall agreement with the TES and Mars Express results, as well as the GCM models, however its spatial distribution looks different from the GCM predictions, with evidence for an enhancement at low latitudes toward the evening side. The inferred mean H_2O_2 abundance is 15 ± 10 ppb, which is significantly lower than the June 2003 result [Encrenaz, T., Bézard, B., Greathouse, T.K., Richter, M.J., Lacy, J.H., Atreya, S.K., Wong, A.S., Lebonnois, S., Lefèvre, F., Forget, F., 2004. Icarus 170, 424–429] and lower than expected from the photochemical models, taking in account the change in season. Its spatial distribution shows some similarities with the map predicted by the GCM but the discrepancy in the H_2O_2 abundance remains to be understood and modeled.

Keywords: Mars; Mars, atmosphere; Atmospheres, composition; Infrared observations

1. Introduction

High spatial and spectral resolution ground-based imaging spectroscopy of Mars in the infrared is a powerful tool for monitoring the narrow spectral signatures, due to the very low surface pressure, of atmospheric gases. This has been illustrated, in particular, by the maps of water vapor and hydrogen peroxide recorded with the Texas Echelon Cross Echelle Spectrograph (TEXES), mounted on the NASA Infra Red Telescope facility (IRTF) at Mauna Kea Observatory in June 2003 (Encrenaz et al., 2004, 2005). These maps were obtained by comparing weak individual transitions of H_2O_2 and HDO, respectively, with a neighboring CO_2 weak line of comparable depth; mixing ratios were inferred from the direct ratio of the lines depths. At the time of these observations ($L_s = 206°$), both species were found in global agreement with the GCM predictions and (in the case of H_2O) with the TES results. The first reported detection of H_2O_2 by Clancy et al. (2004), corresponding to $L_s = 251°$, was also in agreement with the models and with the TEXES map. However, a previous search for H_2O_2, performed with the same instrument in February 2001 ($L_s = 110°$) failed to detect this species and led to a stringent upper limit, hardly compatible with the photochemical models (Encrenaz et al., 2002). Recently, following an earlier suggestion by Atreya and Gu (1995), Atreya et al. (2006, 2007) have pointed out that elec-

* Corresponding author.
E-mail address: therece.encrenaz@obspm.fr (T. Encrenaz).

0019-1035/$ – see front matter
doi:10.1016/j.icarus.2008.01.022

trostatic discharges appear during dust storms and dust devils, when dusty grains are highly charged, and could lead to strong and localized sources of hydrogen peroxide. A spatial and seasonal monitoring of H_2O_2 thus appears important, in order to better understand its temporal variations.

On November 30–December 1, 2005, we have obtained a new map of H_2O_2, still using the TEXES instrument. We now have constraints on the H_2O_2 abundance and spatial distribution for several values of L_s, which allow us to test photochemical models under different seasonal conditions (Lefèvre et al., 2006). In addition, a new water vapor map, also obtained during our 2005 run using a HDO transition, can also be compared with global climate models and with space data, in particular from MAWD/Viking, TES/MGS and Mars Express.

In this paper, we present the new maps of H_2O and H_2O_2 obtained in 2005 with TEXES. Section 2 describes the observations, the modeling and the retrieval method. The H_2O_2 and H_2O maps are presented in Sections 3 and 4, respectively. In Section 5, we compare our results with LMD/GCM simulations coupled with a photochemical model.

2. Observations and modeling

2.1. Observations

Observations of Mars were performed on November 30–December 1, 2005, using the Texas Echelon Cross Echelle Spectrograph (TEXES; Lacy et al., 2002) at the NASA Infra Red Telescope facility (IRTF). This instrument covers the 5–25 μm range with a spectral resolving power of about 8×10^4 and a spatial sampling of 0.3683 arcsec (pixel size). Our spatial resolution, after binning, was about 1.5 arcsec. We have selected the 1235–1243 cm^{-1} spectral interval (8.05–8.10 μm), partially used in our 2003 run, which contains transitions of H_2O_2 and HDO.

At the time of our observations, the diameter of Mars was 17 arcsec. The solar longitude was 332° (end of southern summer). The latitudes of the sub-solar point (SSP) and the sub-terrestrial point (STP, at the disk center) were 11° S and 19° S, respectively. The local time of the STP was 11:00 am. Due to the planet's rotation, its western longitude ranged, between the beginning and the end of the observations, from 65° to 95° W on the first night and from 55° to 85° W on the second night. The western longitude of the SSP ranged from 45° to 75° W on the first night and from 35° to 65° W on the second night. The radial velocity was +9 km/s, corresponding to a Doppler shift of -0.038 cm^{-1}. As in the case of our 2003 observations, we used a 1.1×8 $arcsec^2$ slit and we mapped alternatively the northern and southern hemispheres of Mars (with regard to the celestial pole), by orienting the slit along the N–S celestial axis and by moving it from west to east by 0.5 arcsec steps. Each individual map was recorded in about 10 min. The northern and southern maps, measured in the continuum, were recentered by superimposing the limbs of each individual map, both for the north and the south hemispheres. Then, the final maps were built using the difference in declination coordinates of the northern and southern components, and checking the adjustment of their limb position. The data reduction and radiance calibration are described in Encrenaz et al. (2002, 2004). Calibration of the TEXES spectra follows the radiometric method commonly used for millimeter and submillimeter observations (Rohlfs and Wilson, 2004). Calibration frames consisting of 3 elements (black chopper blade, sky and low emissivity chopper blade) are systematically taken before each observing sequence, and the difference (black–sky) is taken as a flat field; a complete description of the procedure can be found in Lacy et al. (2002). As in the case of our 2003 run, the data were not corrected for telluric absorption in order to preserve the original S/N ratio.

In the 1235–1243 cm^{-1} range, the strongest lines of the spectrum are absorption lines due to H_2O and CH_4 in the terrestrial atmosphere. In addition, the spectrum shows doppler-shifted martian lines due to CO_2 (in particular at rest frequencies of 1235.67 and 1241.58 cm^{-1}, see Fig. 1), HDO (at 1236.3 and 1239.95 cm^{-1} rest frequencies) and H_2O_2 (at 1241.53 and 1241.61 cm^{-1} rest frequencies, see Fig. 1). It should be noted that the CO_2 lines and the HDO line are not visible in the spectrum of the terrestrial atmosphere; the strongest terrestrial absorption lines are due to H_2O and CH_4. The H_2O_2 lines and the 1239.95 cm^{-1} HDO transition, associated to the CO_2 1241.55 cm^{-1} transition, have been used to retrieve the H_2O_2 and H_2O maps in our previous studies (Encrenaz et al., 2004, 2005).

Fig. 1 shows a part of the spectrum recorded on December 1, between 1241.45 and 1241.75 cm^{-1}, where the two strongest H_2O_2 lines are observed, in addition to martian CO_2 lines. This spectrum is averaged over a region centered around 55° S latitude and 0° W longitude, covering the [30°, 80° S] latitude range and the [45°, 315° W] longitude range. As shown in Fig. 2, this area, close to the southern evening limb of the planet, corresponds to a maximum depth of the martian CO_2 lines; this maximum is the combination of the high airmass and the relatively large temperature contrast between the surface and the atmosphere. The same area has been used for spectral summation on both nights, but the longitude of the corresponding area are shifted by 10° between the two nights.

Fig. 3 shows a map of the continuum radiance at 1241.4 cm^{-1}. The maximum radiance (33 $erg/s/cm^2/sr/cm^{-1}$) is located south of the SSP and corresponds, for a surface emissivity of 1.0, to a maximum brightness temperature of 275 K. It can be seen that the maximum radiance is about two times lower than the one measured in June 2003 (Encrenaz et al., 2005). This change is mostly due to the seasonal change (southern summer in 2003, nearly equinox in 2005): maximum brightness temperatures, extracted from the European Martian Climate Database (EMCD; Lewis et al., 1999; Forget et al., 2006) are 320 K and 285 K for the 2003 and 2005 runs, respectively.

Other continuum measurements, obtained during the first night of our run, lead to a similar map. In Section 5.1, we discuss this result in comparison with the predictions of the EMCD.

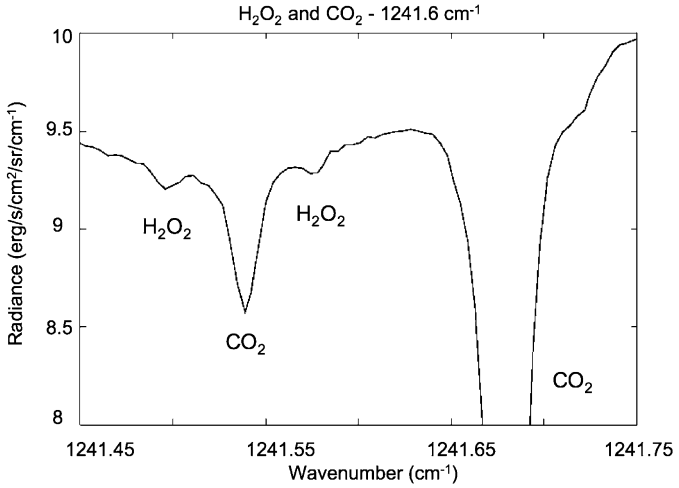

Fig. 1. The raw TEXES spectrum at 1241.45–1241.75 cm^{-1} (December 1, 2005). The two martian CO_2 lines (at 1241.54 and 1241.68 cm^{-1}) and the two H_2O_2 lines (at 1241.49 and 1241.57 cm^{-1}) are Doppler-shifted by -0.038 cm^{-1}.

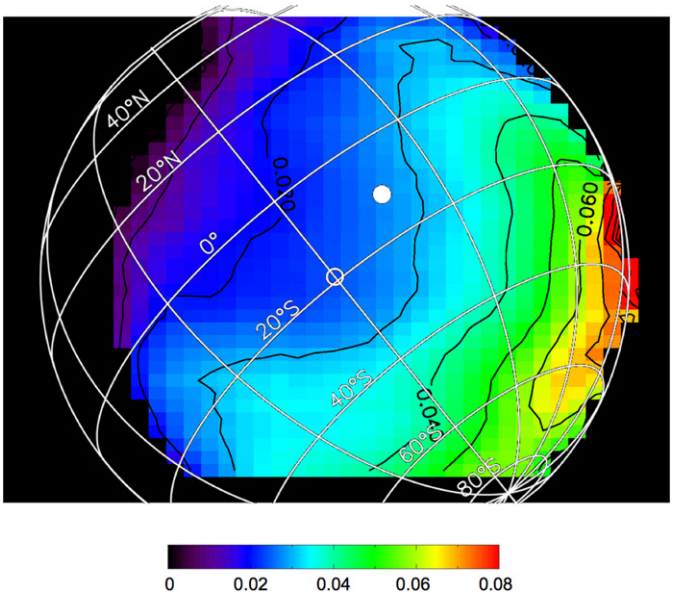

Fig. 2. Map of the CO_2 line depth at 1241.58 cm^{-1} (rest frequency). It can be seen that the area of maximum contrast is close to the southern evening limb of the planet. This area has been used for the spectral summation shown in Fig. 1. The longitude of the central meridian is 70(±15)° W.

2.2. *Retrieval of gas mixing ratio*

We have modeled the martian lines using a line-by-line radiative transfer code (Encrenaz et al., 2004, 2005). Spectroscopic data were taken from the GEISA data bank (Jacquinet-Husson et al., 2005). In addition, the line positions and the intensities of the weak CO_2 isotopic lines, not listed in GEISA, were calculated using the work of Rothman (1986) and Toth (1985). In order to model the mean spectrum (Fig. 1), we used a surface temperature of 250 K (corresponding to the continuum radiance), an airmass of 2.5, and we extracted from the EMCD database the thermal profile corresponding to the area covered by our selection. We then adjusted the surface pressure in order

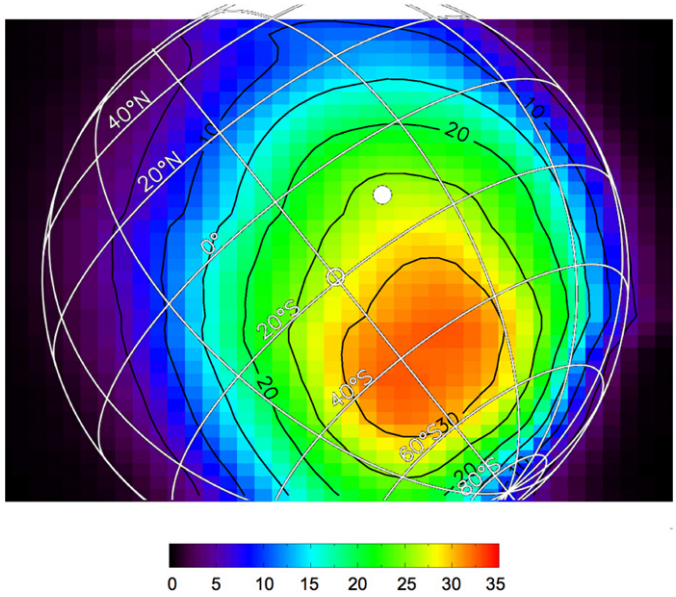

Fig. 3. The TEXES map of the continuum radiance at 1241 cm^{-1} (December 1). The SSP is indicated with a white dot. The longitude at the central meridian is 70(±15)° W. For a surface emissivity of 1.0, the maximum continuum radiance of 33 $erg/s/cm^2/sr/cm^{-1}$ would correspond to a surface temperature of 275 K; a radiance of 10 $erg/s/cm^2/sr/cm^{-1}$ would correspond to a surface temperature of 235 K.

to fit the depth of the weak CO_2 lines. The GCM thermal profile corresponds to $T(z = 0) = 215$ K, $T(z = 10$ km$) = 190$ K and $T(z = 20$ km$) = 175$ K. As the CO_2 line is weak (as well as the H_2O_2 and HDO lines), the temperature above 20 km has no effect on the line modeling. Best fits were obtained for surface pressures of 6 mbar on November 30 and 5 mbar on December 1.

In the case of the November 30 data, we selected a CO_2 transition (Fig. 4) at 1235.64 cm^{-1} (Doppler-shifted position). It is a doublet of 2 superimposed transitions at 1235.675 cm^{-1} and 1235.676 cm^{-1} (rest frequencies), respectively, which have both an intensity of 0.903×10^{-25} cm molec^{-1}, and respective energy levels of 673.45 and 673.43 cm^{-1}. This CO_2 line was used for comparison with the HDO transition at 1236.295 cm^{-1} (rest frequency) which has an intensity slightly larger than the one at 1240 cm^{-1}, used in Encrenaz et al. (2005). The fits are shown in Section 3 (1241 cm^{-1}, Fig. 5) and Section 4 (1236 cm^{-1}, Fig. 7b).

For retrieving mixing ratios out of our data, the ideal method would consist in retrieving the temperature profile in each point of the disk and using it for modeling the spectrum. This method, however, would require us to rely upon model results to estimate the surface and atmospheric temperatures. As in the case of our previous studies (Encrenaz et al., 2004, 2005), we have chosen another method by which we infer the mixing ratios from the line depth ratios of the absorption lines. Indeed, as discussed below, calculations show that when the lines are optically thin, the line depth mixing ratio has only a weak dependence upon the atmospheric and geometric parameters. Here the line depth is defined as the fractional absorption at the line center. This quantity is calculated from the ratio of the radiance

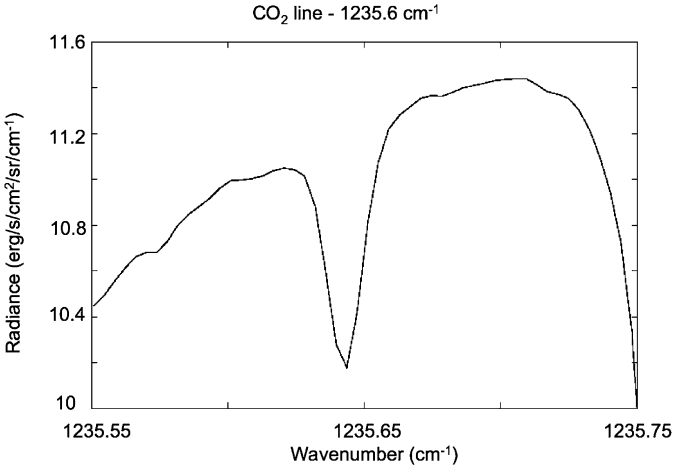

Fig. 4. The raw TEXES spectrum of the martian CO_2 line at 1235.65 cm^{-1}, used for the retrieval of the HDO/CO_2 ratio for the November 30 observations.

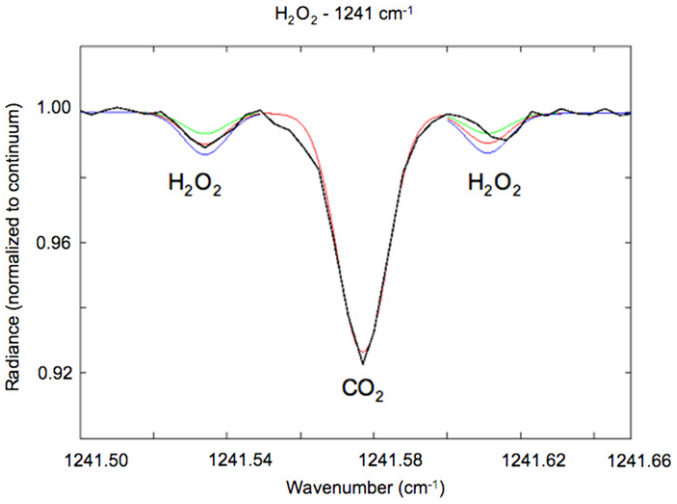

Fig. 5. The TEXES spectrum between 1241.5 and 1241.66 cm^{-1} corrected for the continuum slope, compared to synthetic models. Model parameters are described in the text. Black: TEXES data, corrected for the doppler shift. Models: $H_2O_2 = 10$ ppb (green), 15 ppb (red), 20 ppb (blue). There is a slight misfit in the position of the H_2O_2 line at 1241.61 cm^{-1}, possibly due to an uncertainty in the spectroscopic parameters. There is a weak absorption around 1241.555 cm^{-1}, which corresponds to 1241.517 cm^{-1} in the raw spectrum (Fig. 1). As the same feature was also present in our 2003 raw spectrum (Encrenaz et al., 2004; Fig. 3) we believe it is not associated to the martian spectrum, but probably of telluric or instrumental origin. (For interpretation of the references to color in this figure legend, the reader is referred to the web version of this article.)

at the line center divided by the half-sum of the continuum on each side of the line.

The lines we have been using in our present and past studies have depths of a few percent and are optically thin, with the exception of the CO_2 line at 1241.6 cm^{-1} which has a depth of 7.5%. Taking into account the instrumental convolution, the optical depth at the line center is about 0.5. The departure from the optically thin regime is expected to induce an uncertainty which needs to be quantified. In order to validate our method, we have built a grid of spectra corresponding to a large range of parameters. We have modeled all the lines which have been used in the present study (CO_2 at 1235.6 and 1241.6 cm^{-1}, H_2O_2 at 1241.53 and 1241.61 cm^{-1}, HDO at 2136.3 cm^{-1}). We have allowed for variations of the mixing ratio by a factor of 2, the airmass from 1.0 to 2.5, and the lower atmospheric temperature gradient by a factor of 2. The temperature contrast between the surface temperature and the $T(z = 0)$ temperature was allowed to range from 0 to 30 K. Calculations show that, in all cases, for both H_2O_2 and HDO transitions, for a given mixing ratio, the variation of the line depth ratio, computed with the different models, is always less than 30%; this uncertainty is indeed not negligible and must be kept in mind when interpreting the maps.

3. H_2O_2 mapping

On December 1, we observed the H_2O_2 doublet around 1241 cm^{-1}, previously used in Encrenaz et al. (2004) to retrieve the H_2O_2 map. This doublet, at rest frequencies of 1241.53 and 1241.61 cm^{-1}, respectively, has the advantage of bracketing the weak CO_2 line at 1241.58 cm^{-1}, which can be used to retrieve the $[H_2O_2]/[CO_2]$ ratio. The spectrum, however, looks different from the one observed in June 2003 (Encrenaz et al., 2004) because the Doppler shift is negative, while it was positive in 2003. As a result, there is no more contamination by the strong telluric CH_4 absorption at 1241.8 cm^{-1} (Fig. 1, to be compared with Fig. 3 of Encrenaz et al., 2004).

Fig. 5 shows the TEXES spectrum in the same area as for Fig. 1, corrected for the continuum slope (by adjusting the continuum on each side of each line) and compared to synthetic models. It can be seen that the best fit is obtained for a H_2O_2 mixing ratio of 15 ppb, a value significantly lower than the value retrieved in June 2003 in the region of maximum S/N (Encrenaz et al., 2004); this region was located in the vicinity of the sub-solar point, in the [10° N, 35° S] latitude range and the [100°–150° W] longitude range. Note, however, that in June 2003 (before opposition) this area corresponded to the morning side; in December 2005, after opposition, the maximum CO_2 line depth (and hence the maximum sensitivity) is observed in the evening side.

As shown in Fig. 5, there is a slight mismatch (by about 0.009 cm^{-1}) of the position of the 1241.62 cm^{-1} line, attributed to H_2O_2. This effect was already observed in our previous Encrenaz et al. (2004) analysis, and was also present on another doublet component at 1234.05 cm^{-1}. Because over half a dozen H_2O_2 transitions were identified, we think that these small discrepancies do not question the H_2O_2 identification. The offsets might be due either to instrumental effects or to uncertainties in the spectroscopic parameters of the ν_6 H_2O_2 band.

Fig. 6 shows the retrieval of the H_2O_2 map. The map of the H_2O_2 mixing ratio (Fig. 6b) is inferred from the ratio of the mean depth of the two H_2O_2 lines (Fig. 6a) by the CO_2 line depth (Fig. 2). In Section 5, we discuss the comparison of the H_2O_2 map with the predictions generated by the photochemical model coupled with the LMD/GCM.

In order to validate our method further, we have selected two other points in the map for which we have extracted the EMCD thermal profile. The first one is the STP at the disk cen-

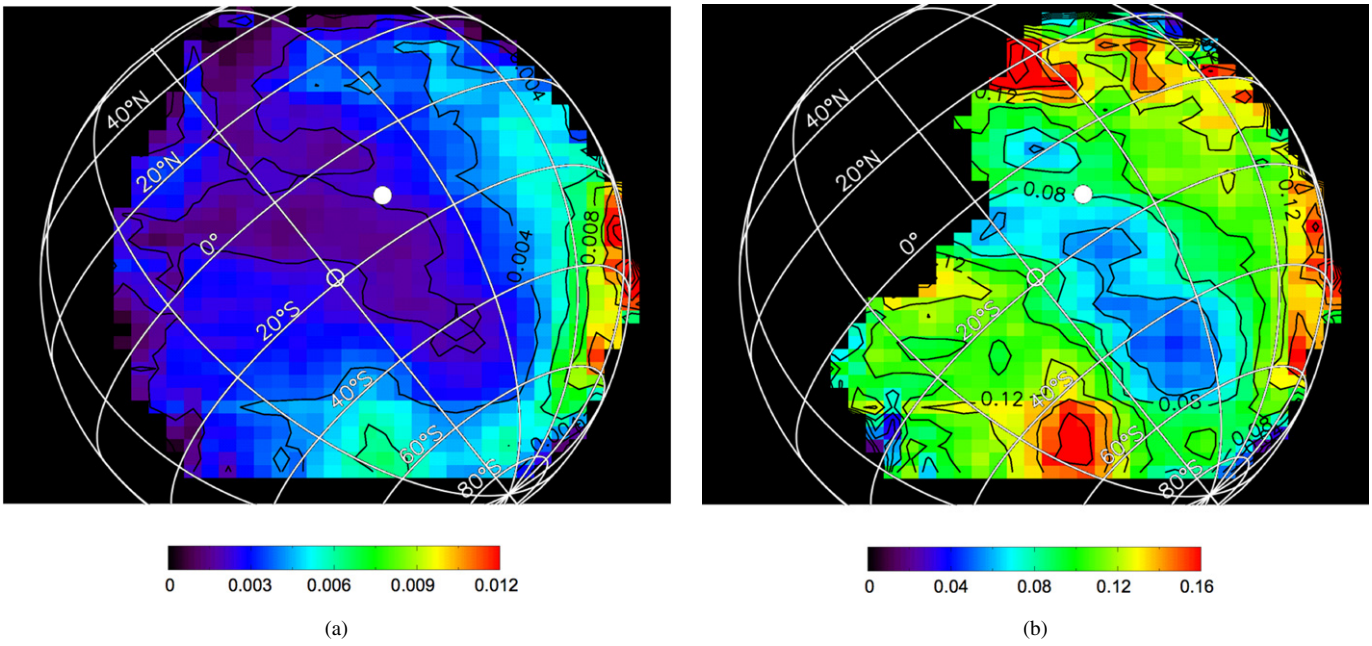

(a) (b)

Fig. 6. Retrieval of the H_2O_2 mixing ratio map (December 1 data): (a, left) map of the H_2 line depth (average of the 1241.53 and 1241.61 cm^{-1} lines); (b, right) O_2 the H_2O_2/CO_2 line depth ratio [(b)/(a)]. As shown in Fig. 5, an H_2O_2 mixing ratio of 15 ppb corresponds to an H_2O_2/CO_2 line depth ratio of 0.13 (green area). The SSP is indicated with a white dot. The longitude at the central meridian is 70(±15)° W. (For interpretation of the references to color in this figure legend, the reader is referred to the web version of this article.)

ter (75° W, 20° S), with an airmass of 1.0. The second one is on the evening limb (15° W, 10° N) near the equator, with an airmass of 2.5. For a H_2O_2 mixing ratio of 15 ppb, the line depth ratio is lower than the one in the selected area by 22% in the first case, and by 6% in the second case. We thus confirm the error analysis mentioned above (Section 2.2) and conclude that our maps provide a measurement of the H_2O_2 mixing ratio within an accuracy better than 30%. Finally, as mentioned in our previous work (Encrenaz et al., 2004), the mean vertical mixing ratio inferred of H_2O_2, as retrieved by our analysis, is not really meaningful: most of photochemical models predict a non-uniform mixing ratio with, near the surface, an effective scale height smaller than the mean atmospheric scale height. A more physical parameter is the column density inferred from the mean mixing ratio. In the present case, a mixing ratio of 15 ppb corresponds to a column density of 3×10^{15} cm^{-2}.

4. HDO mapping

As in the case of our earlier study (Encrenaz et al., 2005), the water vapor map was retrieved from the mapping of a HDO transition, assuming a constant D/H ratio over the martian disk. This assumption is discussed in more detail below.

The HDO abundance was measured using two different transitions: (1) 1236.3 cm^{-1} (November 30), and (2) 1240.0 cm^{-1} (December 1). The 1240.0 cm^{-1} transition was already used in the analysis of the 2003 data (Encrenaz et al., 2005). However, in the present case, the negative Doppler effect shifts the line in the close vicinity of a terrestrial H_2O absorption line centered at 1240 cm^{-1}. Thus, we have not considered this transition in our analysis.

The other HDO transition has a rest frequency of 1236.295 cm^{-1} and is doppler-shifted to a frequency of 1236.26 cm^{-1}. Its intensity, at standard temperature and pressure conditions, is 3.84×10^{-24} cm molec^{-1}, and its energy level is 469 cm^{-1} which, under martian conditions, corresponds to an intensity about twice stronger the transition used in June 2003 ($I = 2.42 \times 10^{-24}$ cm molec^{-1}, $E = 577$ cm^{-1}). Fig. 7 shows (a) the raw spectra of the HDO transition (the CO_2 nearby transition used for comparison is shown in Fig. 4), in the selected area (same as in Fig. 1) as defined in Section 2.1, and (b) the fit of the HDO line, ratioed to the nearby continuum, compared with synthetic models. The atmospheric parameters (the same as described in Section 2.2) allow us to fit also the 1235-cm^{-1} CO_2 line. It can be seen that the best fit is obtained for a H_2O mixing ratio of 150 ppm, which corresponds to a column density of 8.3 pr-μm.

As in Encrenaz et al. (2005), we assume a constant HDO/H_2O mixing ratio of 5 times the terrestrial value, as derived by Krasnopolsky et al. (1997). This assumption may be incorrect, as fractionation effects are expected to be associated to water condensation and sublimation, leading to a change in the D/H ratio. These effects have been studied by Mumma et al. (2003), Montmessin et al. (2005) and Novak et al. (2007). Montmessin et al. (2005) have calculated the expected D/H ratio as a function of latitude and seasonal cycle. Their analysis shows that for $L_s = 332°$, between 60° S and 30° N latitudes, the D/H ratio is between 4.8 and 5.0 times the terrestrial value. However, calculations show a significant gradient of the D/H ratio between mid-northern latitudes and the north pole, with values ranging from 5 times down to 2.5 times the terrestrial value. The error associated with our hypothesis is thus less than 4% for all lati-

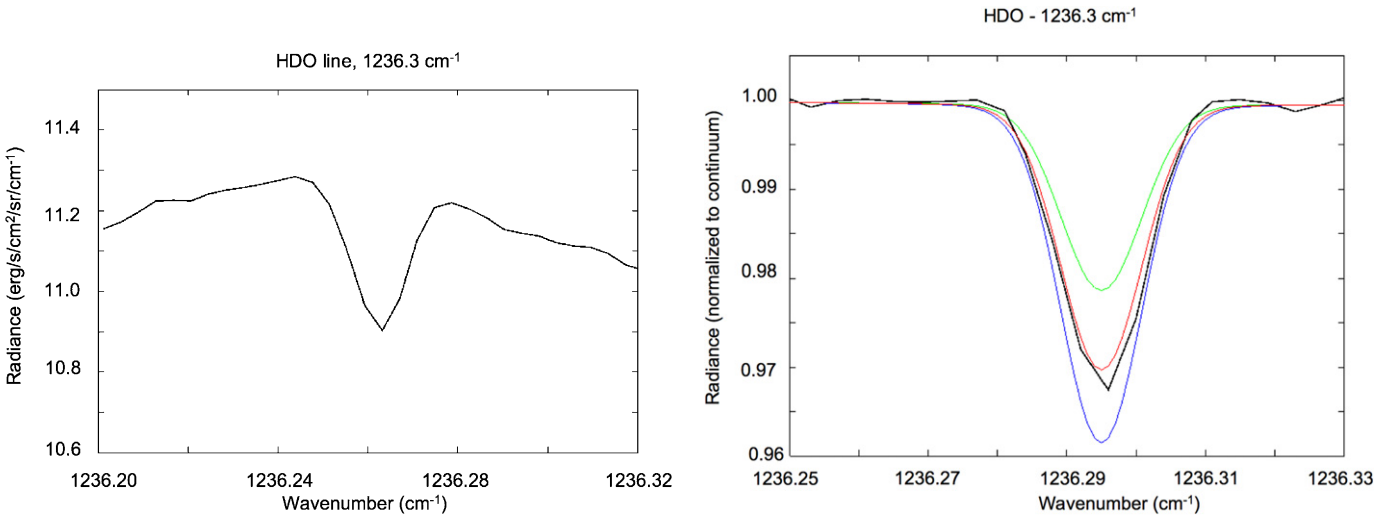

(a) (b)

Fig. 7. (a, left) The raw TEXES spectrum at 1236.26 cm^{-1} (HDO line). (b, right) The TEXES HDO line at 1236.3 cm^{-1}, corrected for the Doppler shift and ratioed to the nearby continuum, compared with synthetic models. Model parameters are described in the text. Black: TEXES data. Models: HDO = 100 ppm (green), 150 ppm (red), 200 ppm (blue). (For interpretation of the references to color in this figure legend, the reader is referred to the web version of this article.)

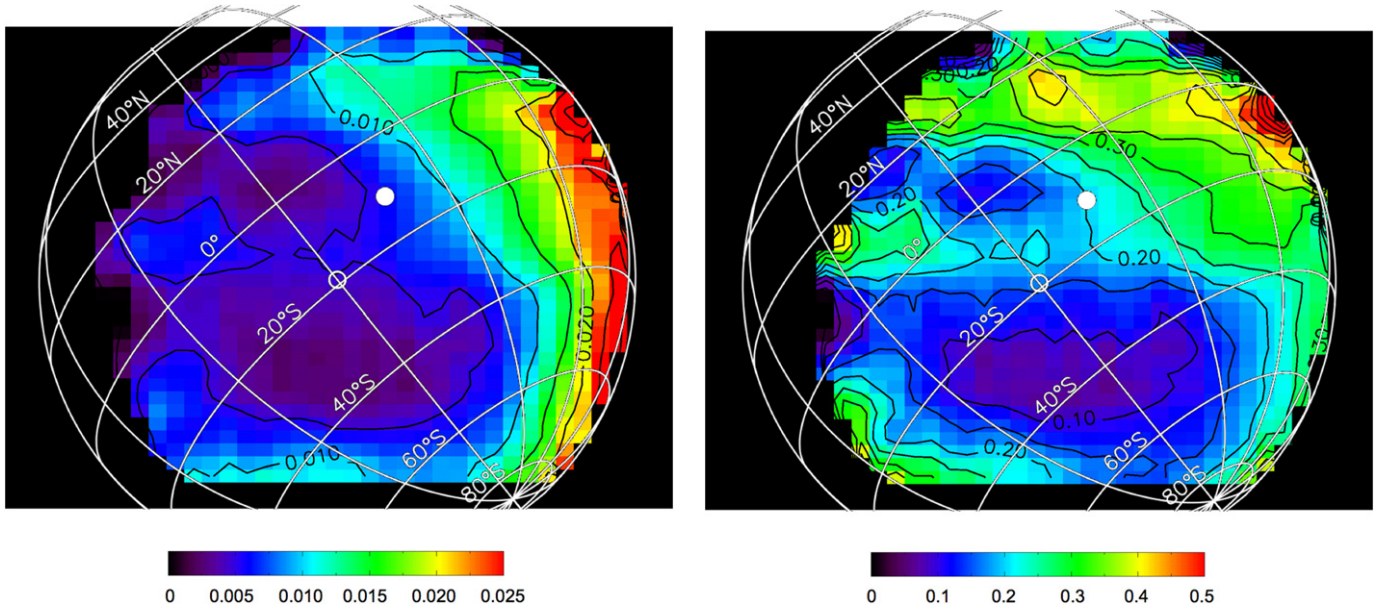

(a) (b)

Fig. 8. Retrieval of the H_2O mixing ratio map (November 30 data): (a, left) map of the HDO line depth at 1236.3 cm^{-1}; (b, right) the HDO/CO_2 line depth ratio. An H_2O mixing ratio of 150 ppm corresponds to an HDO/CO_2 line depth ratio of 0.3 (green area). The SSP is indicated with a white dot. The longitude at the central meridian is 80(±15)° W. (For interpretation of the references to color in this figure legend, the reader is referred to the web version of this article.)

tudes except at southern latitudes higher than 60° S, where our values can be underestimated by as much as a factor 2.

The H_2O mixing ratio map is retrieved using the same method as for H_2O_2, with the 1235-cm^{-1} CO_2 line being used for comparison. Fig. 8 shows (a) the map of the HDO line depth and (b) the map of the HDO/CO_2 line depth ratio. The map of the 1235-cm^{-1} CO_2 line depth shows a behavior similar to that of the 1241-cm^{-1} CO_2 line (Fig. 2).

As in the case of the H_2O_2 map (Section 3), we have modeled the HDO and CO_2 spectra in the two other specific locations used for the November 30 data (the STP at [75° W, 20° S] and the second point at [15° W, 10° N]). As a result, the mixing ratios calculated from the model are lower than our inferred mixing ratios by 8% in the first case and 2% in the second case, respectively. These departures are well within the 30% accuracy mentioned above (Section 2.2).

5. Discussion

The season of our observations ($L_s = 332°$) is known to be quite peculiar. For instance, during the previous martian

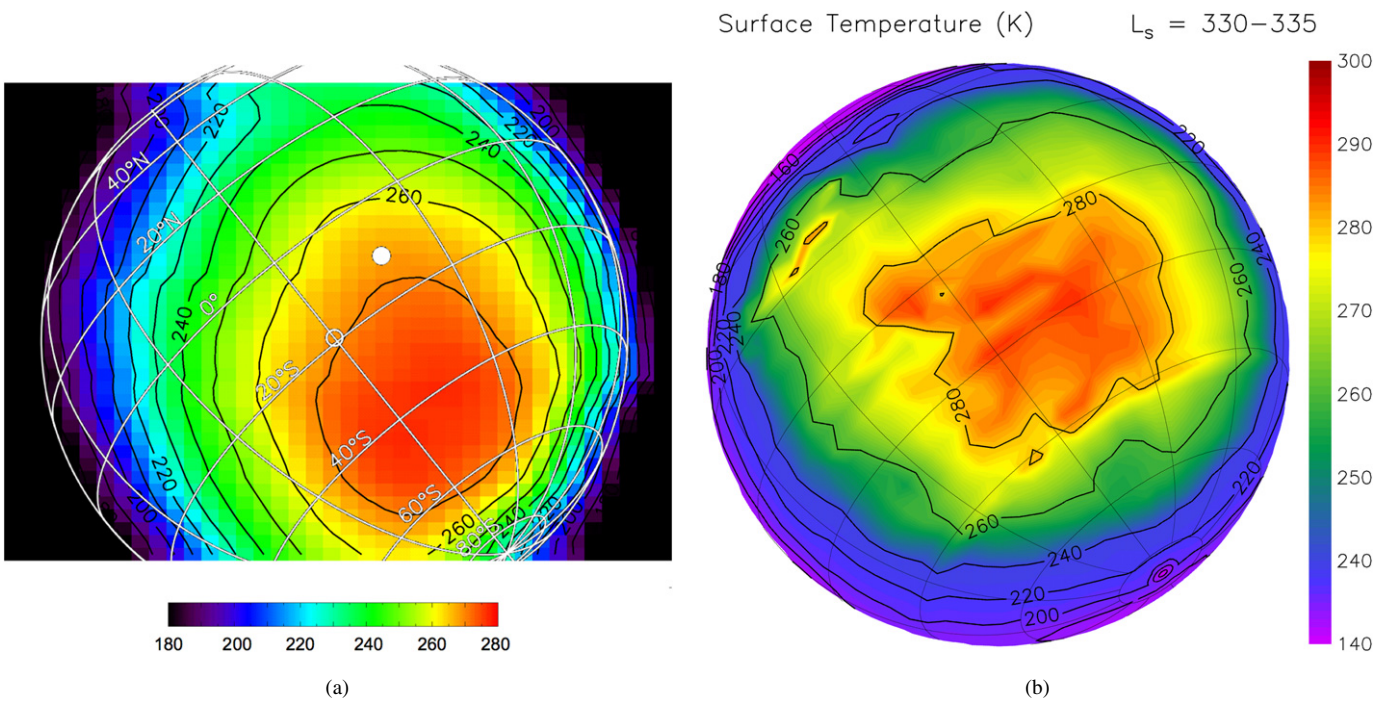

Fig. 9. (a, left) The surface temperature map measured by TEXES from the continuum at 1241 cm^{-1}, assuming an emissivity of 0.95; (b, right) the surface temperature map predicted by the GCM for $L_s = 330°$–$335°$. The local hour at the central meridian is 12:00. The longitude of the central meridian is 60° W.

year (January 2004) the Thermal Emission Spectrometer (TES) detected a raise of dust opacity just before this period. At $L_s = 332°$, this led to a relatively dusty atmosphere everywhere between the south pole and about 30° N, with absorption dust optical depth at 1075 cm^{-1} scaled at 610 Pa around 0.4 (corresponding to a visible dust optical depth around 1). Unfortunately, TES was no longer operational at the time of our observations. Dust observations performed with Themis aboard Mars Odyssey (M.D. Smith, personal communication) suggests that a similar event took place in November–December 2005, although it was not as strong as the year before. Nevertheless, the presence of airborne dust significantly warmed the atmosphere which must have been devoid of water ice clouds during daytime, as also suggested by the Themis data. In such conditions, water vapor was not trapped in the lower atmosphere because of condensation, and it is likely that H_2O as well as HDO was well mixed vertically. The water vapor column density is thus simply linked to the H_2O vertical mixing ratio.

5.1. Surface temperatures

The mapping of the surface temperature, from the continuum measurement, is very straightforward and the two maps obtained on November 30 and December 1 (Fig. 3) show a similar behavior. The maximum surface temperature (Fig. 9a) is observed at a latitude of about 40° S and at about the same longitude as the SSP.

Fig. 9b shows the surface temperature as predicted by the LMD/GCM for $L_s = 330°$–$335°$. It can be seen that the location of the maximum observed temperature (30 degrees south of the SSP) is different from that predicted by the GCM. Similarly, comparison with the TES observations at 2 pm obtained at the same season the previous martian year (and with which the GCM differs by less than 10 K everywhere) suggest that the maximum surface temperature should be between 30° and 0° S rather than between 55° and 25° S.

We also note that the observed TEXES continuum brightness temperatures at 1241 cm^{-1} are colder than the predicted surface temperature (~290 K). This could be partly due to some uncertainty in the absolute calibration of the TEXES data. However, it is also likely that the brightness temperatures at 1241 cm^{-1} does not correspond to the kinetic surface temperature because of (1) non-unit surface emissivity effect and (2) the absorption and emission of colder airborne dust particles. On the one hand, according to TES measurements, the surface emissivity at 1240 cm^{-1}, is close to 0.95 rather than 1.0 (Smith et al., 2000). Assuming a surface emissivity of 0.95, the inferred maximum temperature is about 277 K. One the other hand, as mentioned above, at the time of our observations, the martian atmosphere was probably relatively dusty, with vertical absorption dust optical depth at 1075 cm^{-1} (measured by TES for the same L_s over previous martian years) up to 0.4. The dust absorption is thought to be weaker at 1241 cm^{-1} but it is not negligible. Assuming the dust optical single scattering properties from Forget (1998), one can estimate that the absorption dust optical depth τ at 1241 cm^{-1} is about half the absorption at 1075 cm^{-1}, and that it could have reached 0.2. Assuming a surface temperature of 280 K and a mean airborne dust temperature of 220 K, one can estimate the order of magnitude of the apparent cooling effect of dust on brightness temperature at 1241 cm^{-1} (scattering is neglected): −3.5 K for $\tau = 0.1$, −7 K for $\tau = 0.2$, −10 K for $\tau = 0.3$, −13 K for $\tau = 0.4$, −16 K for $\tau = 0.5$. Values above $\tau = 0.2$ are shown to illustrate the cooling of dust for oblique viewing angle and/or in low topography regions (higher

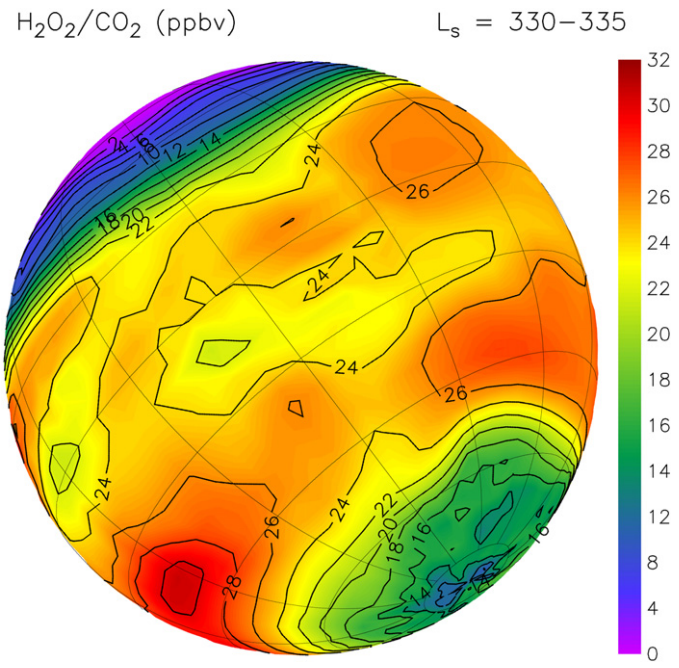

Fig. 10. The H_2O_2 mixing ratio as predicted by the GCM for conditions close to our observations. The longitude at the central meridian is 60° W. The local hour at the central meridian is 12:00.

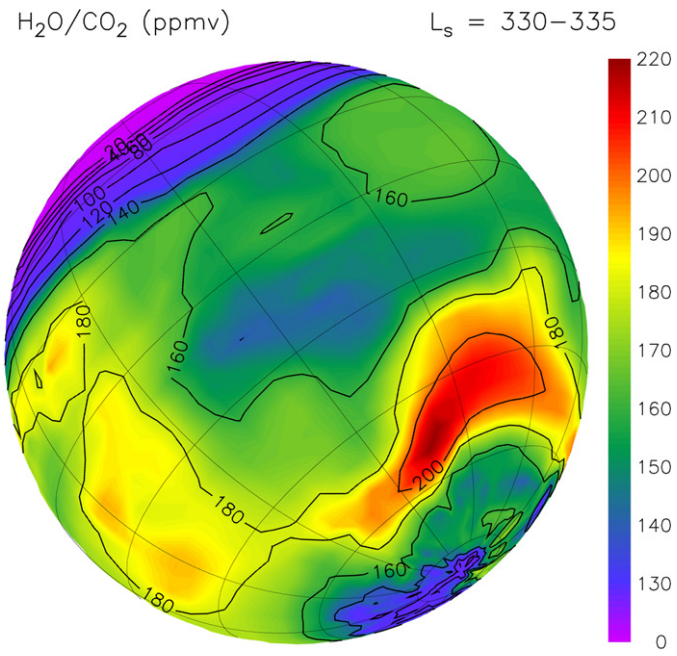

Fig. 11. The distribution of the water vapor mixing ratio, as predicted by the GCM for conditions close to our observations. The longitude at the central meridian is 60° W. The local hour at the central meridian is 12:00.

air mass). One could add that, on the dayside, increasing the dust opacity also tends to decrease the actual kinetic temperature of the surface because of the absorption of solar radiation by the dust.

Can the effect of dust explain the disagreement in horizontal distribution between our observations and both the GCM predictions and the TES observations? That would require a relatively dusty atmosphere north of 30° S and clearer conditions southward in order to have a maximum of brightness temperature around 40° S rather than 20° S. We note that visible images recorded in November and December 2005 report the appearance of a dust event in the northern hemisphere above Chryse on November 23, 2005; however such a localized event may not have been sufficient to account for the temperature map observed with TEXES.

5.2. H_2O_2 map

The H_2O_2 mixing ratio observed in December 2005 ($L_s = 332°$) is significantly lower than the one inferred in July 2003 ($L_s = 206°$), and its spatial distribution is very different. The maximum value is about 15 ppb while it was 40 ppb in 2003; its distribution is more or less spread over the disk in 2005, with a clear minimum along a meridional stripe in the southern hemisphere, while it peaked in a single location, close to morning limb and equator, in 2003. The low value recorded in 2005 was also confirmed by Clancy (2006, private communication) who inferred an upper limit of 15 ppb from disk-integrated submillimeter observations in November 2005.

Fig. 10 shows the H_2O_2 map as expected from a photochemical coupled with the LMD/GCM for the conditions of our observations ($L_s = 330°$–$335°$). The photochemical calculations (Lefèvre et al., 2004) have been adjusted (taking into account the GCM parameters) in order to optimize the agreement on the water vapor abundance between the GCM and the TES and PFS/Mars Express data along the whole seasonal cycle (Fouchet et al., 2007). The maximum value of H_2O_2 predicted by the GCM is about 30 ppb around [120° W, 40° S), while our maximum, not far from this area ([90° W, 50° S] on the TEXES map), is only 16 ppb.

While our 2003 observations were in a good agreement with the GCM predictions, we are now, as in 2001, in a situation where the observed H_2O_2 abundance is lower than the predictions. We note that our 3 data sets correspond to 3 different seasons: the H_2O_2 upper limit obtained in February 2001 was derived at the time of northern solstice ($L_s = 110°$), while those of June 2003 corresponded to southern solstice ($L_s = 206°$) and the present ones are close to equinox ($L_s = 332°$). Regarding the spatial distribution of the H_2O_2 abundance, we note that the model does exhibit a meridional stripe of lower intensity, as observed in our data. However the contrast between this minimum and its surroundings is about 25% at most in the model, while it exceeds 50% in our observations. More theoretical work will be needed to resolve the discrepancies between the models and the observations.

5.3. H_2O maps

Fig. 11 shows the expected distribution of the water vapor mixing ratio, as predicted by the GCM (Forget et al., 1999; Montmessin et al., 2004) under the conditions of our observations ($L_s = 330°$–$335°$). The GCM water cycle model used is similar to the one described in Montmessin et al. (2004), although in the simulations used here, the northern water ice polar cap albedo and the clouds microphysics were slightly modified

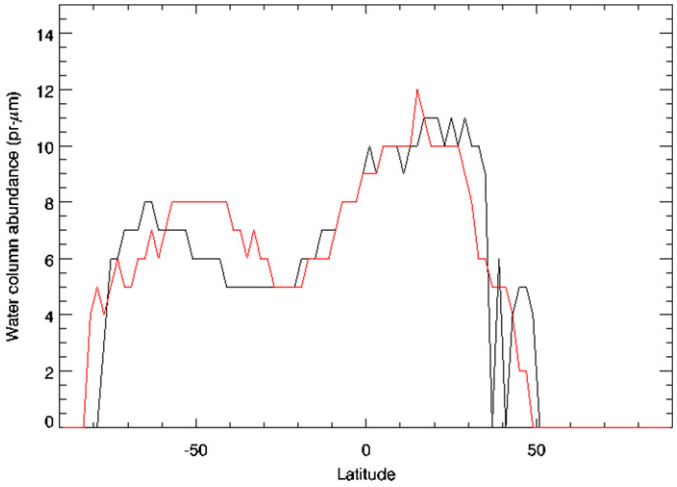

Fig. 12. The water vapor column density, normalized to the 6.1 mbar pressure level, averaged over longitudes, observed by TES for $L_s = 335°$ during MY24 (red curve) and MY26 (black curve). (For interpretation of the references to color in this figure legend, the reader is referred to the web version of this article.)

in order to match (within a few pr-micrometers) the recently revised value of TES water retrieval (M.D. Smith, personal communication) which are now in better agreement with Mars Express observations (e.g., Fouchet et al., 2007). The mean overall mixing ratio shown in Fig. 11 (about 160 ppm) is consistent with our result.

However the spatial distribution of water vapor shows some differences. The GCM map shows a enhancement in the southern hemisphere, with a local maximum around 30° W. In contrast, we observe a maximum H_2O mixing ratio on the evening side around 0°–20° S latitude. Spatial variations, presently not predicted by the models and possibly associated with the local hour, appear to be present in the observed water vapor spatial distribution, and need to be understood and modeled.

Our results can be compared with previous space measurements of the martian water vapor, either from Viking, TES/MGS or Mars Express. The comparison, however, is limited by the fact that space data do not provide instantaneous maps over the martian disk, but measurements along a given meridian at constant local hour. In our model, an H_2O mixing ratio of 150 ppm corresponds to a column density of 8.3 pr-µm. The Viking MAWD data, integrated over longitude, indicate a very low water content (below 10 pr-µm) for all latitudes at $L_s = 335°$. The TEXES results indicate a higher content at some locations (namely on the evening side), however they do not give the longitude-integrated value of the water content.

Fig. 12 shows the latitudinal distribution of the water vapor column density, normalized to a pressure of 6.1 mbar, extracted from the revised TES database (Smith, 2004; Smith, personal communication; Fouchet et al., 2007) for a solar longitude of 335°. Some latitudinal structure is shown, with two maxima around 50°–70° S and 20°–30° M, higher than the Viking values. We see no evidence for these structures in our data. We note also that the TES results show some differences with the latitude distribution predicted by the GCM (Fig. 11). The differences between the TES and Viking results, and between the GCM and the observations, could possibly be attributed to interannual variations.

A comparison can also be done with the results of OMEGA and PFS aboard Mars Express. The $L_s = 337°$ solar longitude was observed early at the beginning of the mission (January 2004). Both OMEGA and PFS find, at the longitude of Olympus Mons (133° W) and in the southern hemisphere, a mixing ratio of about 100 ppb (corresponding to 5.5 pr-µm; Melchiorri et al., 2007; Fouchet et al., 2007). This is consistent with the minimum value of the TEXES map observed in the central part of the southern martian disk. We note, however, that the locations of the observations are different, as the longitude range of Olympus Mons (around 130° W) was not in the TEXES field of view in 2005.

5.4. Conclusions

The TEXES observations have allowed us to obtain quasi-simultaneous maps of the surface temperature, H_2O_2 and H_2O. The main conclusions of this study can be summarized as follows:

- Surface temperature maps are consistent during the two nights. The maximum surface temperature, derived from the 1241.4 cm^{-1} continuum, is 277 K, taking into account an emissivity of 0.95 at 1240 cm^{-1}, which is lower that the GCM predictions. In addition, the location of this maximum is at a higher southern latitude than expected from the model; this effect remains to be understood and modeled;
- The H_2O_2 abundance is found to be lower than the GCM prediction (as in February 2001), but its spatial distribution shows some similarities with the models; in particular, there is evidence for a clear meridional stripe of minimum abundance, which also appears, with less contrast, in the GCM map;
- The water vapor map shows, as the one of hydrogen peroxide, longitudinal variations, with a maximum toward the evening side, which was not predicted by the GCM. The mean water vapor mixing ratio, however, is broadly consistent with GCM predictions and with previous measurements. A precise comparison with previous data sets is however very difficult, because the space data were acquired for a given longitude and at a given local time.

In summary, ground-based infrared mapping of Mars, at high spatial and spectral resolution, is a valuable tool, fully complementary with the space orbiter data. Indeed, these maps provide us with instantaneous and simultaneous maps of H_2O_2 and H_2O, which cannot be obtained from spacecraft, and are important for studying possible diurnal effects and constraining global circulation models.

Acknowledgments

We wish to thank M.J. Mumma for useful comments about this paper. We are grateful to R.T. Clancy for giving us ac-

cess to his result on the H_2O_2 abundance, and to M. Smith for giving us access to the TES data. Observations with TEXES were supported by NSF Grant AST-0205518. T.E. and B.B. acknowledge support from CNRS. T.F. acknowledges support from UPMC. T.K.G. was funded by the Lunar and Planetary Institute under NASA Grant CAN-NCC5-679, and partially by the NASA IRTF.

References

Atreya, S.K., Gu, Z.G., 1995. Photochemistry and stability of the atmosphere of Mars. Adv. Space Res. 16 (6), 57–68.

Atreya, S.K., Wong, A.S., Renno, N.O., Farrell, W.M., Delory, G.T., Sentman, D.D., Cummer, S.A., Marshall, J.R., Rafkin, C.R., Catling, D.C., 2006. Oxidant enhancement in martian dust devils and storms: Implication for life and habitability. Astrobiology (Special Issue on Space Physics, Mars and Life) 6 (3), 439–450.

Atreya, S.K., Mahaffy, P., Wong, A.S., 2007. Methane and related trace species on Mars: Origin, loss, implications for life, and habitability. Planet. Space Sci. 55, 358–369.

Clancy, R.T., Sandor, B.J., Moriarty-Schieven, G.H., 2004. A measurement of the 362 GHz absorption line of Mars atmospheric H_2O_2. Icarus 168, 116–121.

Encrenaz, T., Greathouse, T.K., Bézard, B., Atreya, S.K., Wong, A.S., Richter, M.J., Lacy, J.H., 2002. A stringent upper limit of the H_2O_2 abundance in the martian atmosphere. Astron. Astrophys. 396, 1037–1044.

Encrenaz, T., Bézard, B., Greathouse, T.K., Richter, M.J., Lacy, J.H., Atreya, S.K., Wong, A.S., Lebonnois, S., Lefèvre, F., Forget, F., 2004. Hydrogen peroxide on Mars: Evidence for spatial and temporal variations. Icarus 170, 424–429.

Encrenaz, T., Bézard, B., Owen, T., Lebonnois, S., Lefèvre, F., Greathouse, T.K., Richter, M., Lacy, J., Atreya, S., Wong, A.S., Forget, F., 2005. Infrared imaging spectroscopy of Mars: H_2O mapping and determination of CO_2 isotopic ratios. Icarus 179, 43–54.

Forget, F., 1998. Improved optical properties of the martian atmospheric dust for radiative transfer calculations in the infrared. Geophys. Res. Lett. 25, 1105–1108.

Forget, F., Hourdin, F., Fournier, R., Hourdin, C., Talagrand, O., Collins, M., Lewis, S.R., Read, P., Huot, J.-P., 1999. Improved general circulation models of the martian atmosphere from the surface and above 80 km. J. Geophys. Res. 104, 24155–24176.

Forget, F., Millour, E., Lebonnois, S., Montabone, L., Dassas, K., Lewis, S.R., Read, P.L., López-Valverde, M.A., González-Galindo, F., Montmessin, F., Lefèvre, F., Desjean, M.-C., Huot, J.-P., 2006. The new Mars climate database. In: Forget, F., Lopez-Valverde, M.A., Desjean, M.C., Huot, J.P., Lefèvre, F., Lebonnois, S., Lewis, S.R., Millour, E., Read, P.L., Wilson, R.J. (Eds.), Second Workshop on Mars Atmosphere Modeling and Observations, Granada, Spain, February 27–March 3, 2006. LMD, IAA, AOPP, CNES, ESA, p. 128.

Fouchet, T., Lellouch, E., Ignatiev, N., Forget, F., Titov, D., Tschimmel, M., Montmessin, F., Formisano, V., Giuranna, M., Maturilli, A., Encrenaz, T., 2007. Martian water vapor: Mars Express PFS/LW observations. Icarus 190, 32–49.

Jacquinet-Husson, N., and 41 colleagues, 2005. The 2003 edition of the GEISA/IASI spectroscopic database. J. Quant. Spectrosc. Radiat. Trans. 95, 429–467.

Krasnopolsky, V.A., Bjoraker, G.L., Mumma, M.J., Jennings, D.E., 1997. High-resolution spectroscopy of Mars at 3.7 and 8 μm: A sensitive search for H_2O_2, H_2CO, HCl, and CH_4, and detection of HDO. J. Geophys. Res. 102, 6525–6534.

Lacy, J.H., Richter, M.J., Greathouse, T.K., Jaffe, D.T., Zhu, Q., 2002. TEXES: A sensitive high-resolution grating spectrograph for the mid-infrared. Publ. Astron. Soc. Pacific 114, 153–168.

Lefèvre, F., Lebonnois, S., Forget, F., 2004. A three-dimensional photochemical-transport model of the martian atmosphere. In: Sixth International Conference on Mars, July 20–25, 2003, Pasadena, CA. Abstract 3114.

Lefèvre, F., Perrier, S., Quemerais, E., Montmessin, F., Bertaux, J.-L., Clancy, R.T., Fast, K., 2006. Toward a quantitative understanding of martian ozone. In: Second International Workshop on Mars Atmosphere Modeling and Observations, Granada, February 27–March 3, 2006. Abstract 5.2.2.

Lewis, S.R., Collins, M., Read, P.L., Forget, F., Hourdin, F., Fournier, R., Hourdin, C., Talagrand, O., Huot, J.-P., 1999. A climate database for Mars. J. Geophys. Res. 104, 24177–24194.

Melchiorri, R., Encrenaz, T., Fouchet, T., Drossart, P., Lellouch, E., Gondet, B., Bibring, J.-P., Langevin, Y., Schmitt, B., Titov, D., Ignatiev, N., 2007. Water vapor mapping on Mars using OMEGA/Mars Express. Planet. Space Sci. 55, 333–342.

Montmessin, F., Forget, F., Rannou, P., Cabane, M., Haberle, R.M., 2004. Origin and role of water ice clouds in the martian water cycle as inferred from a general circulation model. J. Geophys. Res. 109 (E10), doi:10.1029/2004JE002284. E10004.

Montmessin, F., Fouchet, T., Forget, F., 2005. Modeling the annual cycle of HDO in the martian atmosphere. J. Geophys. Res. 110 (E3), doi:10.1029/2004JE002357. 03006.

Mumma, M.J., Novak, R.E., DiSanti, M.A., Bonev, B., DelloRussio, N., Magee-Sauer, K., 2003. Seasonal mapping of HDO and H_2O in the martian atmosphere. In: Sixth International Conference on Mars, Pasadena, CA, July 20–25, 2003. Abstract 3186.

Novak, R.E., Mumma, M.J., Villanueva, G., DiSanti, M.A., Bonev, B., Rahon, C.L., Sanstead, C.C., 2007. Seasonal mapping of [HDO/H_2O] in the martian atmosphere. Bull. Am. Astron. Soc. 39. Abstract 24.08.

Rohlfs, K., Wilson, T., 2004. Tools of Radioastronomy. Springer-Verlag, Berlin.

Rothman, L.S., 1986. Infrared energy levels and intensities of carbon dioxide, Part 3. Appl. Opt. 25, 1795–1816.

Smith, M.D., 2004. Interannual variability in TES atmospheric observations of Mars during 1999–2003. Icarus 167, 148–165.

Smith, M.D., Banfield, J.P., Christensen, P.R., 2000. Separation of atmospheric and surface spectral features in Mars Global Surveyor Thermal Emission Spectrometer (TES) spectra. J. Geophys. Res. 105, 9589–9608.

Toth, R.A., 1985. Line positions and strengths of CO_2 in the 1200–1430 cm^{-1} region. Appl. Opt. 24, 261–271.